University of Tehran Press

Journal of the Earth and Space Physics

Homepage: https://jesphys.ut.ac.ir

Vol. 48, No. 4, Winter 2023, P. 21-32
(Research Article)

Airborne Geophysical Data Interpretation of Nkalagu and Abakaliki Regions of the Lower Benue Trough, Nigeria: Implication for Mineral Potentiality

Nnaemeka, E. K.[1] | Ibuot, J. C.[2] ✉ | Obiora, D. N.[3] | Taufiq, S.[4]

1. Department of Physics and Astronomy, Faculty of Physical Sciences, University of Nigeria, Nsukka, Enugu State, Nigeria. E-mail: ejikekings24@gmail.com
2. **Corresponding Author**, Department of Physics and Astronomy, Faculty of Physical Sciences, University of Nigeria, Nsukka, Enugu State, Nigeria. E-mail: johnson.ibuot@unn.edu.ng
3. Department of Physics and Astronomy, Faculty of Physical Sciences, University of Nigeria, Nsukka, Enugu State, Nigeria. E-mail: daniel.obiora@unn.edu.ng
4. Department of Science Education, Waziri Umaru Federal Polytechnic, Birnin Kebbi, Kebbi State, E-mail: suleimantaufiq@gmail.com

(Received: 12 Oct 2021, Revised: 25 Dec 2021, Accepted: 19 April 2022, Published online: 5 March 2023)

Abstract

This study was carried out to delineate possible mineralized zones within Nkalagu and Abakaliki by mapping the structural and hydrothermal alteration zones deduced from the available aeromagnetic and aeroradiometric datasets. Magnetic enhancement techniques such as total magnetic intensity (TMI), reduction to the equator (RTE), analytical signal (AS) and center for exploration targeting (CET) were utilized. The Potassium, Thorium, Uranium, ternary image maps and the K/Th ratio map were produced to aid the interpretation process of alteration areas. The results obtained from the analysis of the airborne magnetic data identified and enhanced the magnetic signatures that reflect the structural features (lineament) of the study area, by revealing the structural trends at the ENE-WSW, NE-SW and WNW-ESE as major trends and NNE-SSW, NW-SE, NNW-SSE as minor trends. The analysis of radiometric data revealed the concentrations of Thorium (eTh), Uranium (eU), and Potassium (%K) concentrations, which were used for the classification of the rock types present in the area. These classifications identified intrusions of basically igneous rocks such as granite, gabbro, rhyolite, diabase, and metamorphic rocks such as quartzite and schist. The areas believed to be hydrothermally altered, aligned NW-SW, NNE-SSW, SE, central potions, and NE borders were identified based on the concentration of radioelements, using K/Th ratio and the ternary maps. Hence, the results obtained from the analysis of the two methods mapped geological structures, geological boundaries, and alteration areas that could be target areas of possible mineral deposits.

Keywords: Aeromagnetic**,** Aeroradiometric, Structures, Alteration Zones, Mineralization.

1. Introduction

Geophysical methods such as magnetic and gravity have been deployed sufficiently in the search for minerals, geothermal energy, and mapping out lithology of different areas in Nigeria. Recently, magnetic and radiometric methods are combined to map out the geology of areas and carry out other geophysical surveys such as geothermal and hydrothermal alteration. Mineral exploration requires interpretation of high-resolution airborne data, which are usually targeted at delineating possible rocks, zones and structures that can serve as hosts for mineral resources (Ajaka et al., 2010; Ekpa et al., 2020; Taufiq et al., 2021). The airborne magnetic and radiometric methods employed in this study have been extensively used in the mineral exploration industries, mainly for the delineation of minerals and metallic deposits in many parts of the world. The magnetic method investigates the subsurface structures based on variations in the earth's magnetic field as a result of the magnetic properties of the underlying rock. According to the literatures, a secondary field is induced when the earth's magnetic field act on magnetic minerals in the crust reflecting the distribution of these minerals (Telford et al., 1990; Hassanein & Soliman, 2009; Abangwu et al., 2021). Magnetic surveying has a broad range of applications like the detection of buried metallic objects and the investigation of geological structures such as faults, contacts, lineaments, sills or dykes (Oha et

Cite this article: Nnaemeka, E. K., Ibuot, J. C., Obiora, D. N., & Taufiq, S. (2023). Airborne Geophysical Data Interpretation of Nkalagu and Abakaliki Regions of the Lower Benue Trough, Nigeria: Implication for Mineral Potentiality. *Journal of the Earth and Space Physics*, 48(4), 21-32. DOI: http//doi.org/10.22059/jesphys.2022.331487.1007368

Publisher: University of Tehran Press.
DOI: http//doi.org/10.22059/jesphys.2022.331487.1007368

Print ISSN: 2538-371X
Online ISSN: 2538-3906

al., 2016; Obiora et al., 2020) whereas radiometric survey is the most applicable to the direct detection of uranium presence. The radiometric method involves the measurement of naturally occurring uranium (U), potassium (K) and thorium (Th), which could be found as trace elements that exist in rock-forming minerals and soil profiles, thereby decaying to give off gamma radiation (gamma rays). The method is very useful in mapping geology by way of distinguishing different rock types since many rocks are naturally radioactive to some certain degrees, radiological hazard assessment, determination of the concentration of radioelements, delineating between sedimentary and basement complex. The method can also assist in identifying intrusive related mineral deposits and potential mineralized zones by knowing that the concentration of rocks is affected by mineralization. This is achieved by mapping hydrothermally altered areas using the K/Th ratio map, which gives a better indication of alteration than simple potassium (K), as the increase in potassium (K) and Thorium (Th) may indicate the presence of gold deposit (Silva et al., 2003), whereas the reduction in Thorium (Th) and the increase in potassium (K) is associated with alteration for most ore deposits (Ostrovskiy, 1975; Dickson & Scott, 1997; Kuforijimi & Christopher, 2017). The variation of magnetic and radiometric mineral composition in rocks due to their differences in lithological setup and mineralization processes make both methods very important in mapping rock lithology, structures and mineral zones because most minerals are usually deposited along with rock contacts or features such as faults or fractures (Rahaman et al., 1988; Ola et al., 2018). Detection of structural trends or magnetic lineaments have been carried out by different authors (Goodhope & Luke, 2013; Opara et al., 2015; Ofoha, 2015; Osinowo & Taiwo, 2020) using aeromagnetic data and landsat data around the study area and delineated different structural trends and lineaments. The need for detailed subsurface information about the structural deformation motivated the current study to map out the geology, linear geological structures (lineaments) and alteration environments that could serve as possible areas of mineral accumulation spots within the study area, by adopting an integrated method of combining airborne magnetic and radiometric dataset, to complement the efforts of previous research works and allow the prediction of targeted areas for detailed exploration work in the search for mineralization within the region of the Lower Benue Trough that has not been extensively explored or researched using the combined methods adopted, compared to other parts of the country. This study is aimed at interpreting the aeromagnetic and aeroradiometric data of Nkalagu and Abakaliki to map out structural and hydrothermally altered zones, which are veins of minerals that may or could aid in delineating zones of possible mineralization in the area.

2. Geology of the study area

The study area is located between latitudes 6° 00' and 6° 30' North and longitudes 7° 30' and 8° 30' East within the lower Benue Trough with a coverage area of about 6050 km^2. The thick sedimentary sequence that underpins the Lower Benue Trough can be traced back to the tectonic processes that followed the separation of African and South American plates in the early Cretaceous (Murat, 1972; Burke, 1996). The Anambra Basin, the Abakaliki Anticlinorium and the Afikpo Syncline are the main component units of the Lower Benue Trough. The sequence belongs to the oldest sediment from the Asu River Group, which sits unconformably on top of the Precambrian basement complex that is made up of granitic and magmatic rocks (Ofoegbu & Onuoha, 1991). The Asu River Group displays outcrops in Abakaliki that are Albian in age and have an approximated thickness of about 2 km (Ofoegbu, 1985). It is made up of argillaceous sandy shales, laminated sandstone units, and small limestones with magnetic volcanic, which interfingers (Nwachukwu, 1972). The shales are fissile and highly fractured, deposited on top of Asu River Group sediments in the area are the Upper Cretaceous Eze-Aku shales. The Turonian Eze-Aku shales consist of nearly 1000 m of calcareous flaky shales and siltstones (Reyment, 1965). They are Turonian in age and are overlain by younger sediments of the Awgu Shale (Coniancian).

These Awgu Shales consist of marine fossil ferrous grey bluish shales, limestones, and calcareous sandstones overlined by the Nkporo Shales (Campanian), which are also mainly marine in nature and has sandstone members. The geological map of the study area is shown in Figure 1.

3. Materials and methods

This study makes use of one sheet each of aeromagnetic and aeroradiometric data sets of Nkalagu (302) and Abakaliki (303). The digitized data was acquired by the Nigeria Geological Survey Agency (NGSA) in Nigeria between the years 2005 and 2009. The data was acquired at a flight altitude of 80 m above the ground surface at tie line spacing of 2000 m. The flight line spacing is 500 m and the digital data was made available on a scale of 1:50,000. The software used for this work are the Oasis Montaj 8.4 software, Surfer 16 software, and the ArcGis.

4. Aeromagnetic Data

In mapping lineaments and structural complexity maps of the area, the data processing started with the production of the Total Magnetic Intensity (TMI) map (Figure 2) using the bi-directional line gridding method. Thereafter, its regional anomaly was separated from the Total Magnetic Intensity to produce the residual magnetic field (Figure 3) adopting polynomial fitting of the second order. This was followed by reduction in the magnetic equator (RTE) given in Figure 4, which was carried out by filtering the residual data in Figure 3 in accordance with the I.G.R.F reduction method using an amplitude correction of inclination 14.1 and declination -2.0 as basic inputs. Since the study area is located in a low latitude region (areas with geomagnetic inclination less than 15˚), in order to return the anomalies back in line with the structures that produce them. The other enhancements of the analytical signal filter (Figure 5), which generated a particular pattern of calculated magnetic anomaly improved map. This defines edges (boundaries) of geological anomalous magnetization distribution, and actually takes the magnitude of the square root of the vertical and horizontal components of the magnetic responses (Geosoft Inc., 1996). The center for exploration Targeting (CET), which is set of algorithms that provide functionalities for enhancement, lineament detection and structural complexity analysis of the potential field data (Core et al., 2009; Holden et al., 2008). The process adopts the method of identifying linear structures within an area through consecutive map byproduct forms of standard deviation (Figure 6a), which estimates magnetic variations. This was followed by the production of a structural map and rose diagram (Figures 6b and 6c) to identify several linear structures and directions of the orientation.

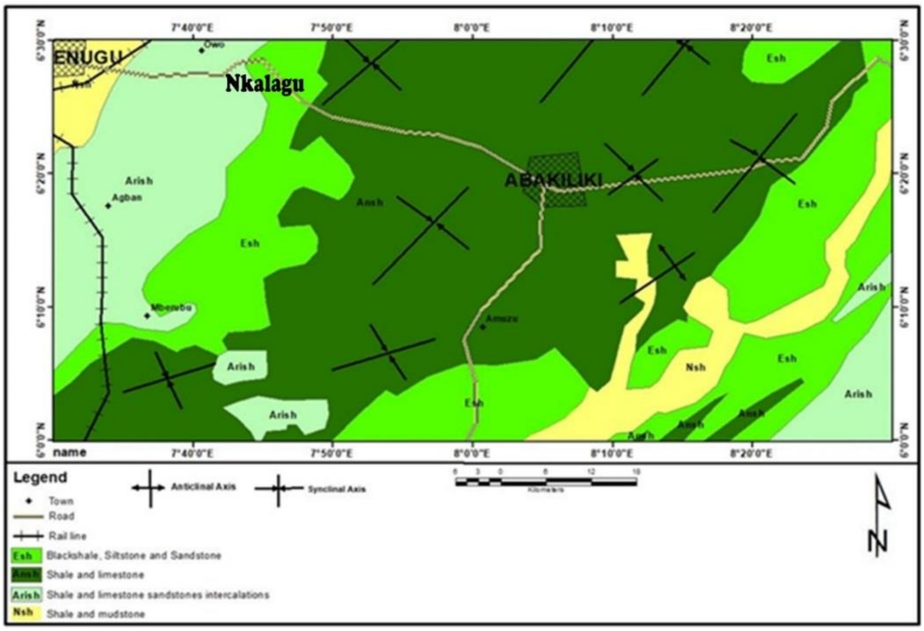

Figure 1. Geological Map of the Study Area.

5. Aeroradiometric Data

The data analysis started with feeding the aero-radiometric data that contain ^{40}K, ^{238}U, and ^{232}Th into Oasis Montaj, and each of these elements was merged separately using the blending method in Grid and Image Geosoft extension (GX) to produce each of the three elements (%K, eTh and eU) concentration maps. The ternary map was made by assigning colors to each of the element abundances. Potassium as red, Thorium as green, and Uranium as blue (Millingan & Gunn, 1997) and combining the three radioelements concentration in the RGB colors using Grid and Image GX of Oasis Montaj. The Ratio map that analyzed the individual anomalies in detail was produced using the Grid math expression builder of the Oasis Montaj. This estimated the ratio map of K/Th as expressed in Equation (1);

$$G_0 = \frac{C_1}{C_2} \quad (1)$$

where G_0 is the total count of the two elements, C_1 is the equivalent of element 1 and C_2 is the equivalent of element 2.

6. Results and Discussion

6-1. Results from aeromagnetic data

The TMI map (Figure 2) is characterized by intensities ranging from 3310 to 33091 nT with high, moderate and low magnitudes. It is clearly represented by the color variations, which enhance the visibility of a wide range of anomalies and their intensities. These variations inherent may be associated with differences in depths and subsurface materials. A dislocation zone is noticed at the southeastern (SE) part representing structural features.

The reduction to the magnetic equator (Figure 4) revealed a similar feature of the faulted zone at the southeastern part as observed in the total magnetic intensity map, but appeared smoother and defined the high and low centers better, because the regional field has been separated from the total magnetic intensity data. Its magnetic intensities range from 12.40 to 93.90 nT corresponding to lows and highs. Application of analytical signal filter on the aeromagnetic data (Figure 5) brought out distinctly the differences in edge extent of geological anomalous magnetization sources. It shows prominent features of high analytical signal amplitude at the southeastern, northwestern, southwestern, central portions, and spots trending northeastern borders of the area. This coincides closely well with the structural deformation of the area because areas of high analytical signal amplitudes are recorded around large areas of large mineral deposits (Liu & Mackey, 1998). The acronyms LMI, MMI, HMI, VLMI, and VHMI on the figures represent low magnetic intensity, medium magnetic intensity, high magnetic intensity, very low magnetic intensity, and very high magnetic intensity respectively. The center for exploration targeting (CET), identified the presence of structures (lineament) within the area, through the standard deviation map (Figure 6a), which measures magnetic variations. The structural map (Figure 6b) was produced to extract the lineaments, this was followed by the production of a rose diagram (Figure 6c) to reveal the frequency and orientation of the extracted lineaments. The extracted structures are aligned in the ENE- WSW, NE-SW, WNW-ESE, NNE-SSW, NW-SE, and NNW-SSE directions, with ENE-WSW, and NE-SW being the most dominant trends in the area as suggested by the rose diagram (Figure 6c). This is in close agreement with earlier studies that suggested Nigeria as having a complex network of fractures and lineaments with dominant trends of NW-SE, NE-SW, N-S and E-W directions. The linear structure that trends NE-SW direction seen from the present study is suggested by Goodhope & Luke (2013) as the continental extension of the known pre-cretaceous oceanic fracture zone and also Charcot and chain fracture zones, which run along the Trough axis beneath the sedimentary cover (Ananaba, 1991; Burke et al., 1971).

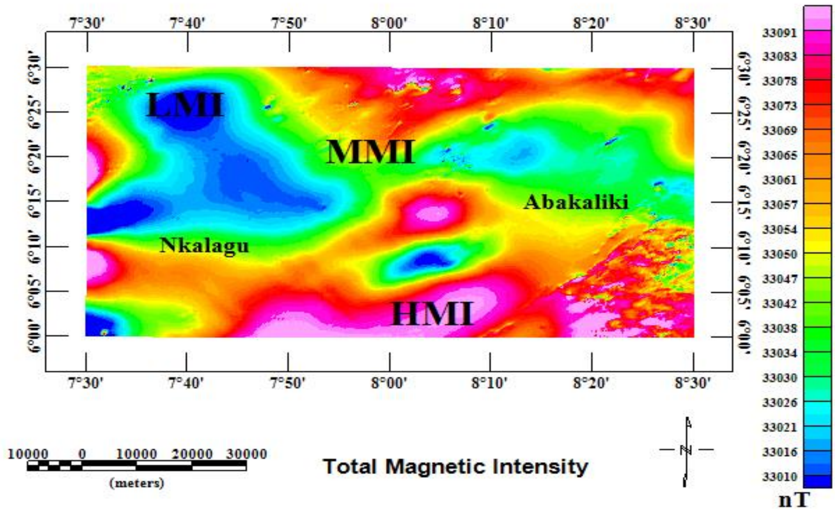

Figure 2. Total Magnetic Intensity Map of the Study Area.

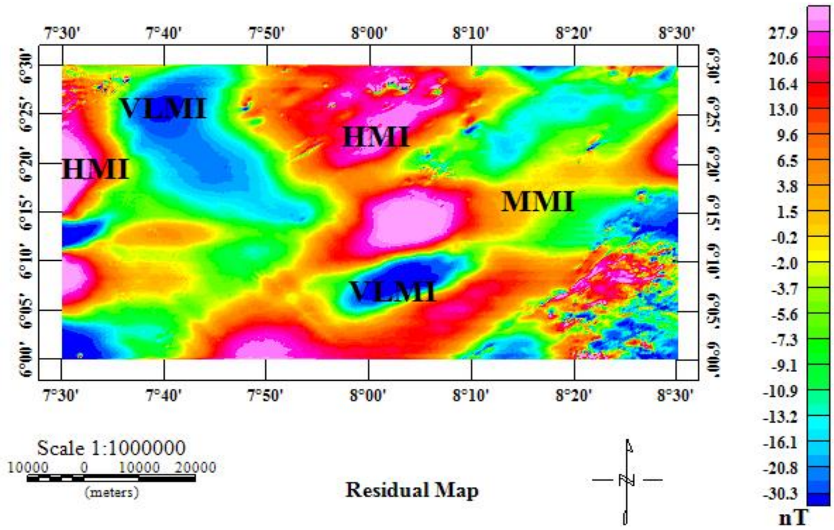

Figure 3. Residual Map of the Study Area.

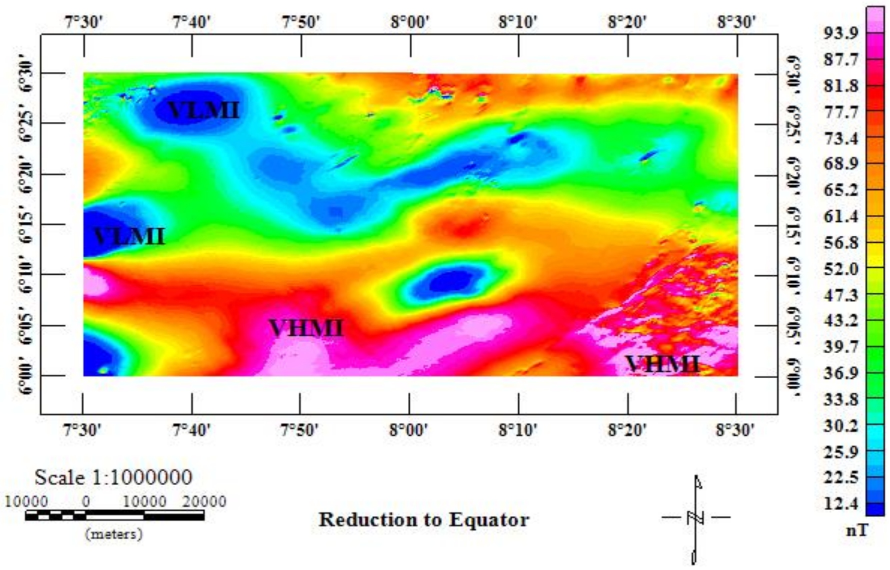

Figure 4. Reduction to the Equator Map of the Study Area.

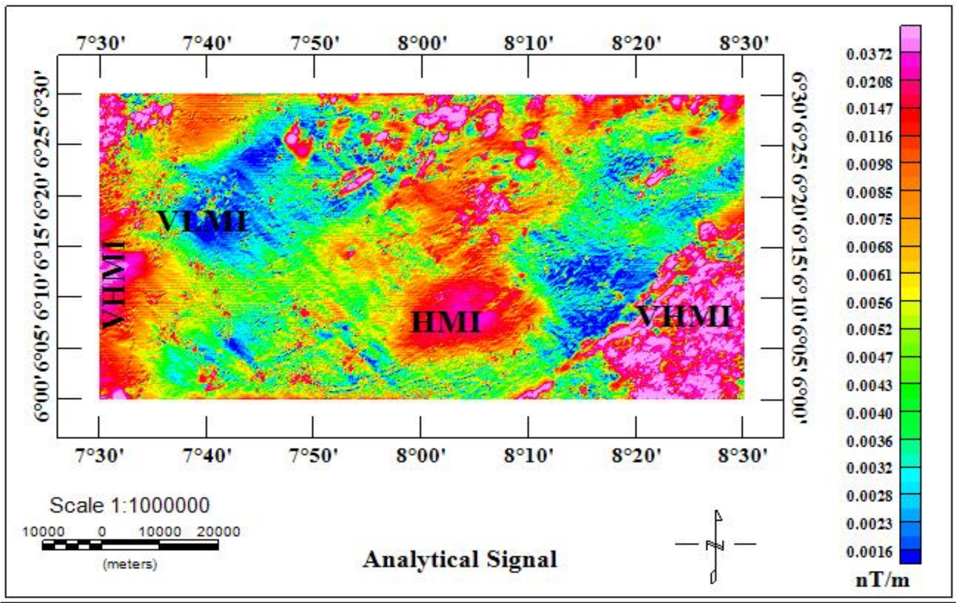

Figure 5. Analytical Signal Map of the Study Area.

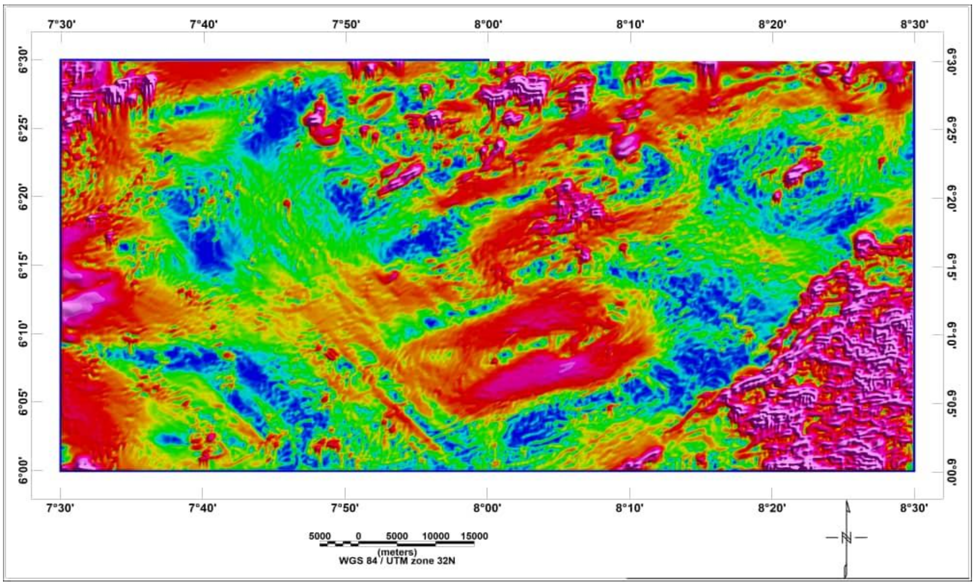

(a)

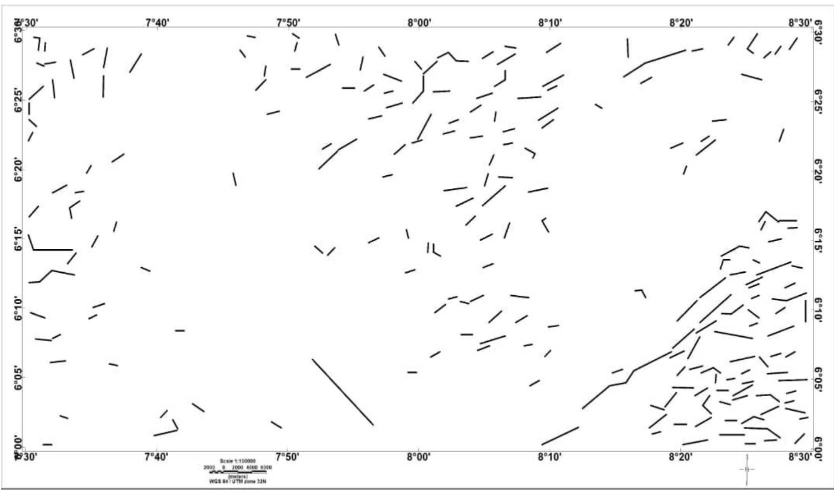

(b)

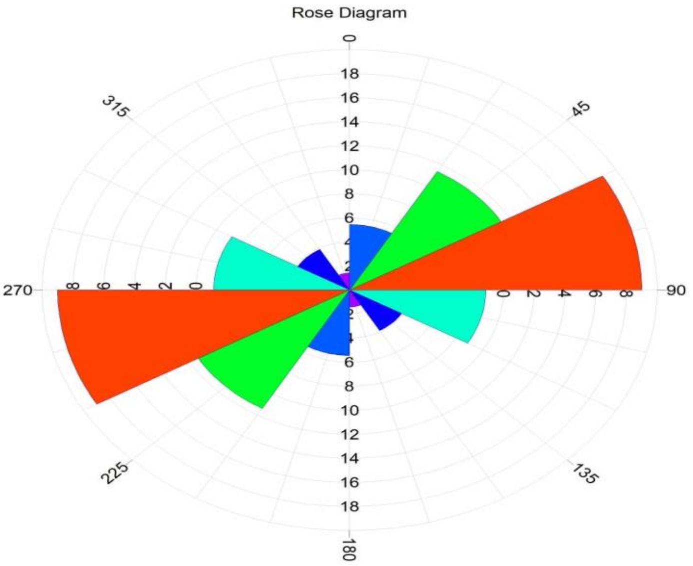

(c)

Figure 6. a) Standard Deviation Map of the Study Area, b) Structural Map of the Study Area, c) Rose diagram (Azimuth frequency) of the lineaments of the study area.

6-2. Results from aeroradiometric Data

6-2-1. %K, eTh, and eU Concentration Maps

The results from the analysis of aeroradiometric data showed concentrations and distribution styles of the principal radioactive elements Potassium (%K), Thorium (eTh), and Uranium (eU) as well as characterizing different rock types and mapping alteration environments within the study area.

6-2-2. Potassium map (%K)

The equivalent Potassium map (Figure 7) revealed three different levels of K-concentrations. The first level (low concentration) represented by blue to a bright green color ranging from 0.10% to 0.44%, is dominant in the north-western (NW) parts of the study area (Owo, Nkalagu, Enugu, Agban and Mbenubu), which is associated with carbonates. The second level (intermediate concentration) represented by orange colors ranging from 0.44% to 0.88% is associated with chemical sedimentary rocks, and the third level (highest concentrations) is represented by pink color ranging from 0.88% to 1.06%, observed at the central portion (Abakaliki and Amuze), southeastern, northeastern and northwestern directions is associated to mafic intrusive rocks.

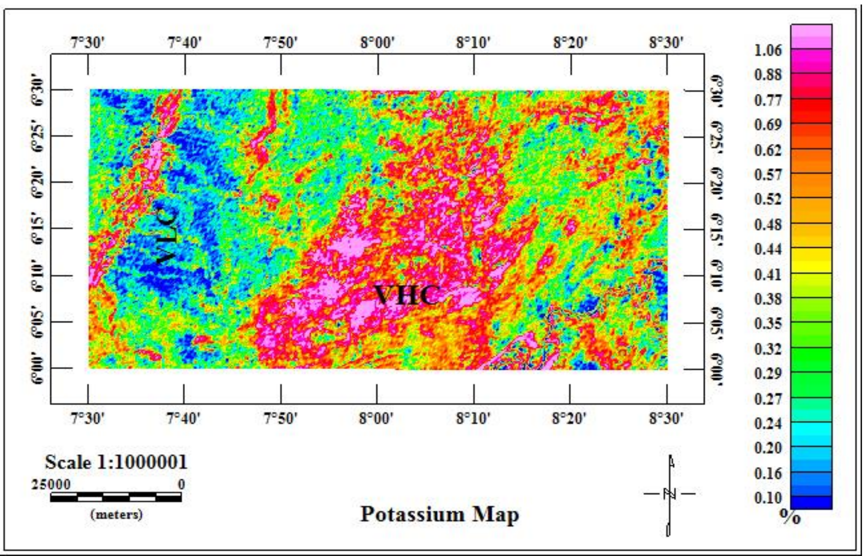

Figure 7. Equivalent Potassium Map of the Study Area.

6-2-3. Thorium map (eTh)

The Thorium equivalent concentration map (Figure 8) showed three distinct regions of Thorium concentrations. The study area is characterized by very high concentration (first region) with values ranging from 19.37 to 21.35 ppm, and moderately high (second region) ranging from 13.97 to 19.37 ppm is associated with felsic intrusive rocks while that of the low concentration (third regions) ranging from 5.48 to 13.97 ppm is associated with felsic extrusive rocks. The high concentration regions are more pronounced at the northern boundaries, central portions and northwestern corner (Enugu and Nkalagu), while the low regions are seen at the western portions (Owo, Agban and Mbenubu).

6-2-4. Uranium map (eU)

The equivalent Uranium concentration map (Figure 9) showed three zones of concentration. The high concentration zones ranging from 4.97 to 5.91 ppm (pink colors) are associated with detrital sedimentary rocks and the moderate concentration zones (red shaded with yellow colors), which is ranging from 3.71 to 4.97 ppm associated with felsic intrusive rocks. The low concentration zones (blue to bright green colors) spanning from 1.62 to 3.71 ppm are metamorphosed sedimentary rocks. This classification was done with respect to radioelement concentrations in different classes of rocks (Killeen, 1979).

6-2-5. Potassium/Thorium Ratio (K/Th) Map

As Potassium (K) is more mobile than Thorium naturally, K/Th ratio anomalies can be indicative of hydrothermal alterations, which are characterized by enrichment in Potassium (K). It is evident from the K/Th map (Figure 10) that the areas characterized by the high content of K/Th concentrations (enrichment in K) represented with AE (alteration environment) seen at the NW-SW, NNE-SSW, and central portions are strong indicators of hydrothermally altered areas with a range from 0.04 to 0.07. However, these alteration environments depict areas with the accumulation of various ore deposits (Ostrovskiy, 1975) found around the area of study. This is because hydrothermal solutions are capable of dissolving and transporting a wide range of metals and salts, which consequently play an important role in ore deposition processes (Boamah, 1993; Manu, 1993).

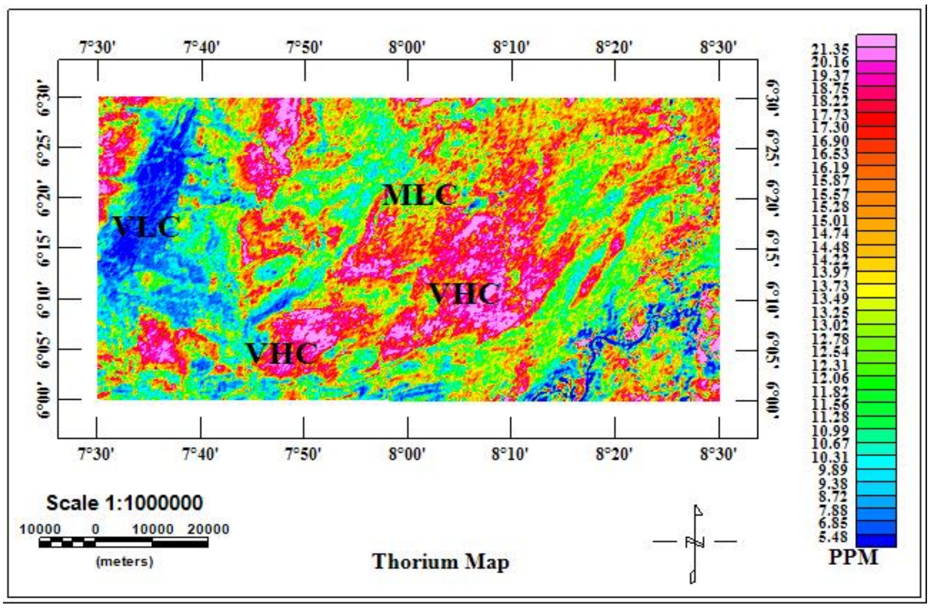

Figure 8. The Equivalent Thorium Map of the Study Area.

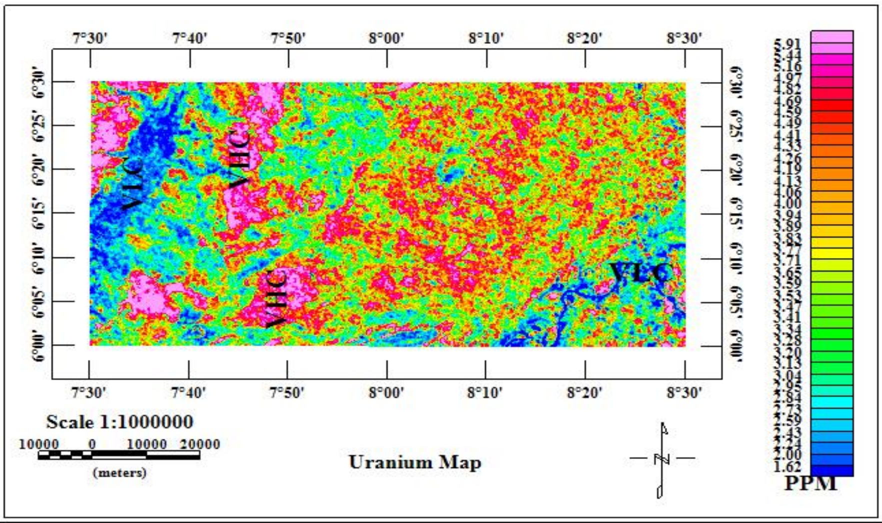

Figure 9. Equivalent Uranium Map of the Study Area.

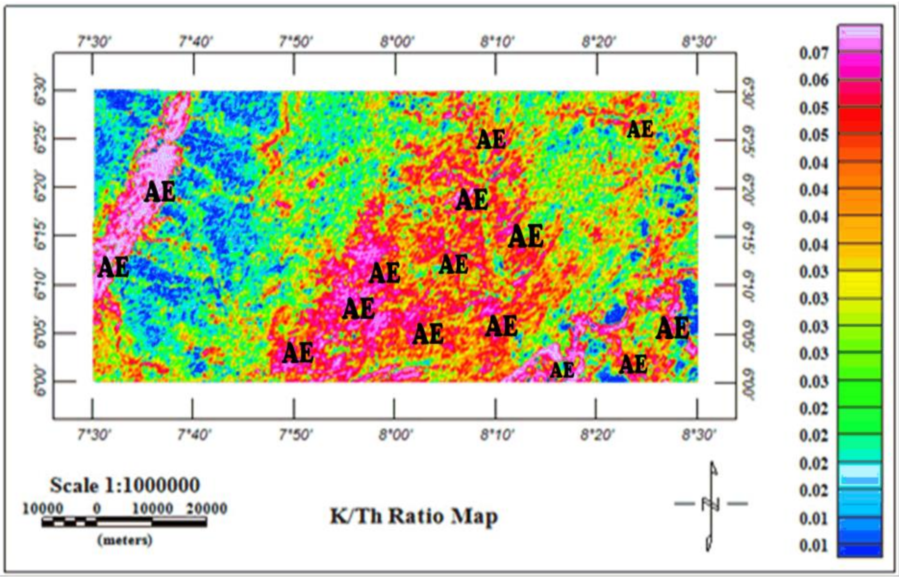

Figure 10. Equivalent Potassium/Equivalent Thorium Map of the Study Area.

6-2-6. The ternary map

Ternary map (Figure 11) revealed combined intensities of Potassium (%K), Thorium (eTh) and Uranium (eU) in red, green and blue respectively. The black color indicates low concentrations of (%K, eTh and eU) seen more at Mbenubu and parts (Owo and Agban). The red color corresponds to high Potassium, low Uranium and low Thorium concentrations. The high concentrations of Thorium, low concentrations of Uranium and Potassium are displayed with green colors. The regions of high Uranium, low Potassium and Thorium concentrations are characterized by blue colors while white color areas are termed regions of high (%K, eTh and eU) concentrations. Additionally, the areas represented with yellow color shows regions of high Potassium, Thorium and low Uranium concentration, which depict possible alteration zones as assigned with AE (Alteration Environment). These areas are observed at the NW-SW, NE borders, central portions and SE directions. This closely agrees with the K/Th ratio map, analytical signal and structural map deduced from the aeromagnetic data. The blue flower color regions could be termed quiet areas.

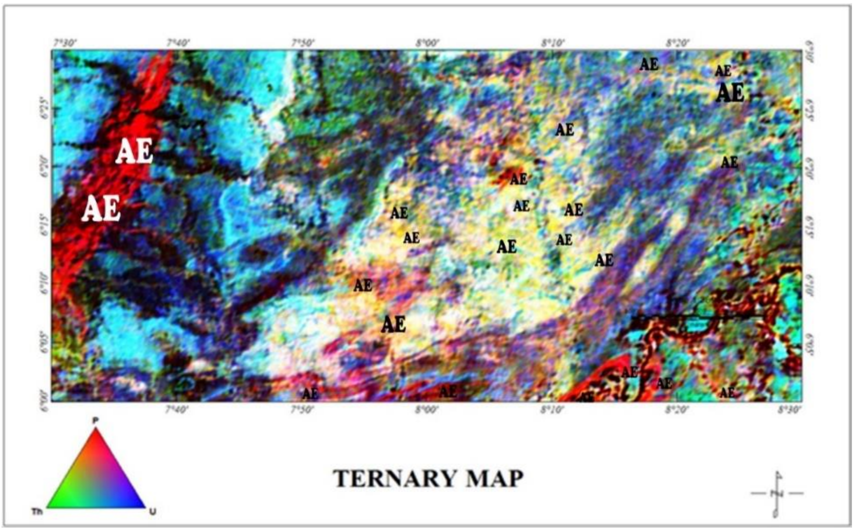

Figure 11. Ternary Map of the Study Area.

7. Discussion of results

The results from the analytical signal and center for exploration targeting revealed clear images of the geologic features by delineating and enhancing the magnetic signatures that reflect the structural features of the study area as revealed by the rose diagram. The structural features trend ENE-WSW, NE-SW, WNW-ESE, NNE-SSW, NW-SE and NNW-SSE directions, and is in close agreement with earlier studies of Goodhope & Luke (2013); Opara et al. (2015) and Ofoha (2015). These lineament directions are veins of mineral accumulation spots, since magnetic minerals are structurally controlled. In radiometric, **t**he immobile nature of Thorium identified igneous intrusions, which intruded within the area at the time of formation, indicating the presence of felsic intrusive and extrusive rocks of rhyolite and granite. The Potassium retained some sedimentary rocks of carbonates, chemical sedimentary rocks of limestone, and mafic intrusive rocks of gabbro. The leaching process of Uranium identified the sedimentary rocks revealed in the geological map of the area, which could be classical sedimentary rocks of sandstone, siltstone, mudstone, shale, and felsic intrusive rocks of granite and metamorphosed sedimentary rocks of schist and quartzite.

The K/Th map identified areas of alteration environments believed to be spots of accumulated ore deposits, which may be found within the area assigned with (AE) on the image map. The ternary map identified areas of combined intensities of the three radioactive elements (^{40}K, ^{238}U, ^{235}U and ^{232}Th) in red, blue and green with further identification of areas of possible alteration environments assigned with (AE) on the image map.

8. Conclusion

The integrated use of airborne magnetic and radiometric datasets assisted in mapping the linear structures, hydrothermally altered zones, types of intrusive bodies, and portions where the combined effects of the three radioactive elements are strong. The linear structures suggested by the rose diagram aligned in the ENE-WSW, NE-SW, WNW-ESE, NNE-SSW, NW-SE, and NNW-SSE. The possible alteration environments suggested by the ratio map of Th/K and the ternary map aligned in the NW-SW, NNE-SSW, and central portions are host areas of mineral accumulation spots, which could aid exploration of base metal minerals. It is also evident from the results that some areas with high magnetic signatures, which reflect the structural patterns of the area coincide with areas of low and high radiometric signatures. Also, the intrusions delineated from the radiometric data closely agree with the types of intrusions delineated by other researchers who have worked in the area using magnetic methods. These intrusions, by implication can destroy hydrocarbons, because, the presence of numerous intrusions is an indication of exceedingly high temperature.

Hence, alterations in the study area may be attributed to structural deformations, this will help in the exploration of economic minerals within the study area.

References

Abangwu, J.U., Obiora, D.N., Ibuot, J.C., & Ekwueme, O.U. (2021) Estimation of Curie point depth and geothermal gradient in parts of the Bida Basin. *Nigeria. Journal of Environmental Engineering and Science*, 17(1), 41-50. doi.org/10.1680/jenes.20.00054.

Ajaka, E.O., & Oyetheiemi, E.O. (2010). Suggesting Areas for Detailed investigation of mineral occurrences in Nigeria for national resources database. *ARPN Journal of Engineering and Applied Sciences*, 5(11), 27-39.

Ananaba, S.E. (1991). Dam sites and crustal mega lineaments in Nigeria. *ITC Journal*, (1), 26-29.

Boamah, D. (1993). Application of soil geochemistry to gold exploration in the Birimian rocks of Ghana. *Unpublished M.Sc. Thesis*, Case study from Demoni/Dankyira area, pp 1-6.

Burke, K.C. (1996). The African plate. *South African Journal of Geology*, 99, 341-409.

Burke, K., Dessauvagie, T.F.J., & White Man, A.J. (1971). Opening of the Gulf of Guinea and Geological History of Benue Depression and Niger Delta. *Nature Phy. Sci*, 233, 51-55.

Core, D., Buckingham, A., & Belfield, S. (2009). Detailed structural analysis of magnetic data – done quickly and objectively, *SGEG Newsletter.*

Dickson, B.L., & Scott, K.M. (1997). Interpretation of aerial gamma ray surveys-adding the geochemical factors. *AGSO Journal of Australian Geology and Geophysics*, 17(2), 187-200.

Ekpa, M.M.M., Ibuot, J.C., Okeke, F., & Obiora, D.N. (2020). Investigation of Subsurface Structures within Parts of Niger Delta, Nigeria, Via Aeromagnetic Data. *Geological Behavior*, 4(2), 66-71.

Geosoft Inc. (1996). OASIS Montaj Version 4.0 User Guide, Geosoft Incorporated, Toronto.

Goodhope, A., & Luke, M. (2013). Structural interpretation of Abakiliki- Ugep, Using Airborne and Landsat Thematic Mapper (TM) Data. *Journal of Natural Science Research*, 3(13), 137-148.

Hassanein, H.I.E., & Soliman, K.S. (2009). Aeromagnetic Data Interpretation of Wadi Hawashiya Area for Identifying Surface and Subsurface Structures, North Eastern Desert, *Egypt. JKAU: Earth Sci.*, 20(1), 117-139.

Holden, E.J., Dentith, M., & Kovesi, P. (2008). Towards the automatic analysis of regional aeromagnetic data to identify regions prospective for gold deposits. *Comput. Geosci*, *34*, 1505-1513.

Killeen, P.G. (1979). Gamma-ray spectrometric methods in uranium exploration–application and interpretation, in P.J. Hood, ed., Geophysics and Geochemistry in Search for Metallic Ores: Geological Survey of Canada, Economic Geology Report 31, 163-230.

Kuforijimi, O., & Christopher, A. (2017). Assessment of aero-radiometric data of Southern Anambra Basin for the prospect of radiogenic heat production. *J. Appl. Sci. Environ. Manag.*, 21(4), 743-748.

Liu, S., & Mackey, T. (1998). Using images in a geological interpretation of magnetic data. *AGSO Research Newsletter*, 28.

Manu, J. (1993). Gold deposits of Birimian greenstone belts in Ghana: Hydrothermal alteration and thermodynamics. Verlag Mainz, Wissenchaftsverlag, Aachen Herstellung: Fotodruck Mainz GmbH Susterfeldstr, 83, 52072 Aachen.

Milligan, P.R., & Gunn, P.J. (1997). Enhancement and presentation of airborne geophysical data. *AGSO Journal of Australian Geology and Geophysics*, 17(2), 63-75.

Murat, R.C. (1972). Stratigraphy and Paleogeography of the Cretaceous and Lower Tertiary in Southern Nigeria, (2nd Eds). *African Geology. University of Ibadan Press*, 251-266.

Nwachukwu, S.O. (1972). The tectonic evolution of the southern portion of the Benue Trough, Nigeria. *Jour. Min. and Geol.*, 11, 45-55.

Obiora, D.N., Dimgba, B.C., Oha, I.A., & Ibuot, J.C. (2020). Airborne and Satellite Geophysical Data Interpretation of the Gubio Area in the Bornu Basin, Northeastern Nigeria: Implication for

Hydrocarbon Prospectivity. Petroleum and Coal, 64(4), 1504-1516.

Ofoegbu, C.O. (1985). A review of the geology of the Benue Trough, *Nig. Journal of African Earth Science*, 3, 293-296.

Ofoegbu, C.O. & Onuoha, K.M. (1991). Analysis of magnetic data over the Abakaliki Anticlinorium of the Lower Benue Trough, Nigeria. *Marine and Petr. Geol.*, 8, 174-183.

Ofoha, C.C. (2015). Geological interpretations inferred from a high resolution aeromagnetic (HRAM) data over parts of Mmaku and environs, South Eastern, Nigeria. *International Journal of Applied Science and Mathematical Theory*, 1(4), 1-15.

Oha, I.A., Onuoha, K.M., Nwegbu, A.N., & Abba, A.U. (2016). Interpretation of high-resolution aeromagnetic data over Southern Benue Trough, Southeastern Nigeria. *Journal of Earth System Science*, 125, 369-385.

Ola, P.S., Adekoya, J.A., & Olabode, S.O. (2018). Source rock evaluation of the southwest portion of the Bornu Basin, Nigeria: IOSR. *Journal of Applied Geology and Geophysics*, 6(3), 27-31.

Osinowo, O.O., & Taiwo, T.O. (2020). Analysis of high- resolution aeromagnetic (HRAM) data of lower Benue trough, Southeastern Nigeria, for hydrocarbon potential evaluation. *Journal of Astronomy and Geophysics*, 9(1), 350-361.

Opara, A.I., Onyekuru. S.O., Essien, A.G., Onyewuchi, R.A., Okonkwo, A.C., Emberga, T.T., & Nosiri, O.P. (2015). Lineament and Tectonic Interpretation over Abakiliki Area. Evidences from Airborne Magnetic and Landsat ETM Data. *International Journal of Research and Innovations in Earth Science*, 2(4), 111-121.

Ostrovskiy, E.A. (1975). Antagonism of radioactive elements in well rock alteration fields and its use in aero gamma spectrometric prospecting. *International Geological Review*, 17, 461-8.

Rahaman, M.A., Ajayi, T.R., Oshin, I.O., Asubiojo, F.O. (1988). Trace element geochemistry and geotectonic setting of lle-ife schist belts prec. Geol. Of Nigeria, GSN pub. Kaduna, 241-256.

Reyment, R.A. (1965). *Aspects of Geology of Nigeria*, Ibadan University Press, Ibadan.

Silva, A.M., Pires, A.C.B., McCafferty, A., Moraes, R.A.V., & Xia, H. (2003). Application of airborne geophysical data to mineral exploration in the uneven exposed terrains of the Rio Das Velhas greenstone belt. Revista *Brasileira de Geociências*, 33(2), 17-28.

Telford, W.M., Geldart, L.P., & Sheriff, R.E. (1990). *Applied Geophysics*. Cambridge. University Press, second edition.

Taufiq, S. Okeke, F.N. Obiora, D.N., & Ibuot, J.C. (2021). Assessment of geothermal potential of parts of Sokoto Basin, Northwest Nigeria using aero-radiometric data. *Modeling Earth Systems and Environment*, 6.